Pepin Nicholas, Charles (Orcid ID: 0000-0001-6200-4937)

Deng Haijun (Orcid ID: 0000-0001-9957-9750)

Zhang Hongbo (Orcid ID: 0000-0003-2584-7139)

Zhang Fan (Orcid ID: 0000-0002-6714-9534)

Kang Shichang (Orcid ID: 0000-0003-2115-9005)

An examination of temperature trends at high elevations across the Tibetan Plateau: The use of MODIS LST to understand patterns of elevation-dependent warming.

Pepin, N.C.[1,2], Deng, H.[3,4], Zhang, H.[2], Zhang, F.[2,5], Kang, S.[6,5,7], Yao, T.[2,5]

1. **Department of Geography, University of Portsmouth, UK**
2. **Key Laboratory of Tibetan Environmental Changes and Land Surface Processes, Institute of Tibetan Plateau Research, Chinese Academy of Sciences, Beijing, China**
3. **Fujian Provincial Engineering Research Center for Monitoring and Assessing Terrestrial Disasters, Fuzhou, 35007, China**
4. **School of Geographical Sciences, Fujian Normal University, Fuzhou, China**
5. **CAS Center for Excellence in Tibetan Plateau Earth Sciences, Beijing 100101, China**
6. **State Key Laboratory of Cryospheric Science, Northwest Institute of Eco-Environment and Resources, CAS, Lanzhou 730000, China**
7. **University of Chinese Academy of Sciences, Beijing, 100049, China**

This article has been accepted for publication and undergone full peer review but has not been through the copyediting, typesetting, pagination and proofreading process which may lead to differences between this version and the Version of Record. Please cite this article as doi: 10.1029/2018JD029798

Abstract

Research has revealed systematic changes in warming rates with elevation (EDW) in mountain regions. However, weather stations on the Tibetan plateau are mostly located at lower elevations (3000-4000 m) and are non-existent above 5000 m, leaving critical temperature changes unknown. Satellite LST (Land Surface Temperature) can fill this gap, but needs calibrating against in- situ air temperatures (T_{air}). We develop a novel statistical model to convert LST to T_{air}, developed at 87 high-elevation Chinese Meteorological Administration stations. T_{air} (daily maximum/minimum temperatures) is compared with MODIS Aqua LST (1330 and 0130 local time) for 8 day composites during 2002-2017. Typically, 80-95% of the difference between LST and T_{air} (ΔT) is explained using predictors including LST diurnal range, morning heating/night-time cooling rates, the number of cloud free days/nights and season (solar angle). LST is corrected to more closely represent T_{air} by subtracting modelled ΔT. We validate the model using an AWS on Zhadang Glacier (5800 m). Trend analysis at the 87 stations (2002-2017) shows corrected LST trends to be similar to original T_{air} trends. To examine regional contrasts in EDW patterns, elevation profiles of corrected LST trends are derived for three ranges (Qilian Mountains, NyenchenTanglha and Himalaya). There is limited EDW in the Qilian mountains. Maximum warming is observed around 4500-5500 m in NyenchenTanglha, consistent with snowline retreat. In common with other studies, there is stabilisation of warming at very high elevations in the Himalaya, including absolute cooling above 6000 m, but data there is compromised by frequent cloud.

1. Introduction

Much recent work has confirmed that rates of warming are dependent on elevation [Rangwala and Miller, 2012; Pepin et al., 2015], and that many high elevation areas, including the Tibetan plateau, have experienced more rapid warming than the global mean over the last 50-60 years (Guo and Wang, 2012; Yan and Liu, 2014; Deng et al., 2017). Many mechanisms have been suggested as playing a part in controlling the spatial patterns of elevation-dependent warming, including snow albedo feedback [Pepin and Lundquist, 2008; Minder et al., 2016; Guo et al., 2016], changes in atmospheric moisture content [Rangwala et al., 2016] and cloud patterns [Duan et al., 2006], the increased sensitivity of temperature to radiative forcing at low temperatures [Ohmura, 2012] and aerosol loading and deposition on snow [Lau et al., 2010]. Many of the mechanisms are the same as those responsible for Arctic amplification [Serreze and Francis, 2006; Serreze et al., 2009].

Our knowledge and understanding of recent temperature changes in many high elevation regions, however, is incomplete. Even in the Tibetan plateau the surface station network is inadequate, being concentrated in the relatively accessible southern and eastern parts of the plateau, mostly below 4000 m. Most stations are in incised valley locations and many are in urban areas. Thus the uncertainty in warming rates from the observational record increases in the higher elevation bands [Yan and Liu, 2014] and lack of high quality in situ temperature data is a serious concern [Lawrimore et al., 2011].

Satellite data in theory can overcome this high elevation gap, because it covers the whole globe. MODIS (Moderate Resolution Imaging Spectroradiometer) is particularly useful since it exists as a more or less complete time series, four times daily since 2000 (Terra Platform) and 2002 (Aqua). MODIS Land Surface Temperature (LST) is increasingly used for a wide range of applications, including climate monitoring where the global standard temperature measurement is 2 m (screen level) air temperature (T_{air}) [Benali et al., 2012; Kustas and Anderson, 2009; Merchant et al., 2013]. However LST is not the same as T_{air}, the former being strongly influenced by the surface characteristics within the pixel which may be an amalgam of differing surface types (e.g. forest, ice

cover, lakes, bare soil). T_{air} is more of a regional mean value, and shows less dramatic temporal and spatial gradients than LST, particularly at high elevation where the transfer of heat into the lower atmosphere through sensible and latent heat fluxes is less efficient. Therefore there are challenges in converting LST to a realistic measure of air temperature at high elevations [Pepin et al., 2016]. Well known issues include contamination by cloud cover [Zhang et al., 2016], the influence of ephemeral snow cover [Shamir and Georgakakos, 2014; Williamson et al., 2017], the role of vegetation in increasing latent heat at the expense of sensible heat [Vancutsem et al., 2010], and timing and spatial differences between the two measurements (point vs pixel).

This paper develops a new statistical model to predict the difference between LST and T_{air} at 87 Chinese Meteorological Administration stations on the Tibetan plateau, and uses the model to correct LST to more precisely represent air temperature. We compare trend patterns in raw and corrected LST with air temperature trends at the stations. While several studies have attempted to obtain an EDW profile on the plateau-wide scale (e.g. Qin et al. 2009, Gao et al. 2018), this approach can hide important regional differences, both in terms of profiles of warming, and therefore the mechanisms responsible. The plateau covers a wide area and includes a range of climates, from monsoonal dominated regions in the south and east, to continental areas in the north, and westerly dominated regimes in the far west. Thus, although we develop our model approach for all stations across the plateau, we apply the model in 3 contrasting mountain regions across the plateau where there are limited in situ weather stations, and where the model works particularly well, to examine local EDW profiles. Focus on small areas where elevation is the dominant cause of spatial variability, potentially discriminates between relevant EDW mechanisms which may be different in different regions. The elevation dependency of raw and corrected LST trends tells us about regional contrasts in high elevation climate change. After a review of past studies in section 2, section 3 explains the data and methods used, section 4 evaluates the success of the model predicting ΔT, and section 5 then examines the trend patterns at the stations before and after correction. The application of this correction to obtain elevational patterns of warming in specific mountain regions is discussed in section 6, before our findings are discussed in a wider context in section 7.

2. Past studies

Although there have been previous attempts to use LST to model high elevation change in the Tibetan plateau, for the most part potential limitations in LST data have remained. Qin et al. (2009) examined elevation patterns in MODIS LST across the plateau and found strongest warming around 4800-6000 m. Although the data was compared with trends from in situ weather stations, it was not corrected for any differences between the two and the period of analysis was also extremely short (2000-2006).

Away from the high elevation context however, there have been numerous studies attempting to use LST to model T_{air} at screen height (1.5 or 2 m) [Benali et al., 2012; Oyler et al., 2015, 2016; Parmentier et al., 2016] since the latter is the focus of climate change assessments [Collins et al., 2013; Comiso and Hall, 2014], being the global standard in climate monitoring [Osborn and Jones, 2014]. Many factors influence the difference between the two measurements [e.g. Benali et al., 2012; Urban et al., 2013; Good et al., 2015, 2016], including the surface characteristics, presence or absence of vegetation, slope aspect, snow cover presence/absence, and geographical location which in turn influences solar loading (latitude) and macroclimate.

LST is a spatial average over the pixel (1 km^2 for MODIS) of the effective surface temperature. The pixel may be an amalgam of different surface types, all with contrasting emissivities and conductivities [Bosilovich 2006; Merchant et al., 2013]. Being a response to surface energy balance,

LST is intrinsically more extreme than T_{air}, usually being colder at night, and often much warmer in the day, especially when the surface receives a lot of direct insolation [Good, 2015, 2016]. The effective surface may be at ground level (rock or snow) or it may be higher (e.g. the forest canopy in vegetated areas). Since a pixel could be a mixture of trees, bare rock and snow, LST can show extreme local variability, especially in mountainous areas [Oyler et al., 2015; Pepin et al., 2016] and it is hard to get a representative measurement or to separate temperatures for various surface types within the pixel [Lundquist et al., 2018].

Most studies in the tropics and lower mid-latitudes [Vancutsem et al., 2010; Mostovoy et al., 2005] have focused on vegetation and its effect on the difference between T_{air} and LST. In general forest vegetation increases the latent heat flux and reduces the extremes of LST in comparison with dry scrubland or arid areas. Forests also raise the effective surface so that LST is measuring the canopy temperature rather than the ground level. Thus LST is generally closer to T_{air} in forested areas due to increased mixing and reduced sensible heating [Mildrexler et al., 2011; Lundquist et al., 2018]. The health of vegetation can be measured by NDVI. More (healthy) vegetation tends to reduce the difference between LST and T_{air}, as does increased humidity (due to increased latent heat flux). Thus the NDVI has been used to estimate the difference [Nemani and Running, 1989; Maeda and Hurskainen, 2014].

In high latitudes and at high elevations, snow is a major control of LST, and in general a snow cover will reduce day time LST much more dramatically than T_{air} [Williamson et al., 2017]. A deep blanket of snow reduces spatial variability in surface temperatures and LST is on average (slightly) colder than T_{air} [Ostby et al., 2014; Westermann et al., 2012; Urban et al., 2013]. Typical differences of 2-3°C (LST colder than T_{air}) have been recorded in Svalbard [Westermann et al., 2012] and 4-5°C in Finnish Lapland [Pepin et al., 2018].

Unidentified cloud in LST images (which are colder than the true surface) and the clear-sky bias (known cloudy days omitted in LST composites) are important limitations in LST/T_{air} comparisons. Cloud bias often leads to an average cold bias of LST below T_{air} in high latitude regions, since clear periods, especially in winter, are commonly colder than cloudy periods [Westermann et al., 2012]. Cloud contamination is also a known issue in the Tibetan plateau, particularly at night when clouds can be difficult to differentiate from the ground surface [Zhang et al. 2016].

Recently, the ability of LST to represent elevation contrasts in temperature has become of interest. Typically as elevation increases, there is a transition from forests, through alpine grassland to bare rock, and finally permanent snow and ice, so all of the previous discussions about vegetation and snow cover have potential relevance. A comparison of lapse rates in Finnish Lapland for LST vs T_{air} showed very little correspondence between the two, because of the elevational gradient in surface types [Pepin et al., 2018]. In the Tibetan plateau in contrast, lapse rates estimated for daily mean temperature from LST were found to show similar seasonal patterns to those based on T_{air} [Zhang et al., 2018a]. There have been relatively few detailed studies of the difference between T_{air} and LST at extreme high elevations above 5000 m, but those that have been performed tend to show increased variance in the difference, a lower correlation between T_{air} and LST, and larger mean differences [Pepin et al., 2016]. Taking all these studies together, clearly a correction is essential before LST can be used to measure elevation-dependent air temperature changes.

3. Data and Methods

Air temperatures are recorded at 87 high elevation stations across the Tibetan plateau (Figure 1). Data is provided by the Chinese Meteorological Administration

(http://www.cma.gov.cn/en2014/climate/) from 1961 to 2017 for most stations (some started later). For comparison with LST we use a shorter period (July 2002- October 2017) for all 87 stations, restricted due to availability of satellite data. We use daily maximum (T_x) and minimum (T_n) temperatures which can occur at any time, but usually T_x is recorded a couple of hours after solar noon, and T_n near dawn (can vary from 0400 to 0800 local standard time depending on season and location). Over most of the plateau the dry atmosphere means that the diurnal cycle in temperature is marked, and it is unusual to record extreme temperatures at other times, although this can occur occasionally in winter under strong advection. Most stations are distributed between 1500 and 4000 m above sea-level, whereas most of the plateau (see Figure 1 b) lies between 4000 and 5000 m above sea-level. Thus there is a mismatch in elevation between stations (mostly in low elevation mountain valleys) and the plateau itself. This reinforces the point that using satellite data to supplement station data in examining temperature trends at higher elevations is potentially helpful.

MODIS LST is recorded 4 times daily at 0130/1330 local solar time (Aqua) and 1030/2230 (Terra). Records start in January 2000 (Terra) and July 2002 (Aqua). LST is derived at 1 km^2 resolution and was downloaded from ORNL DAAC (https://modis.ornl.gov/) using the global subsetting tool version 6 (ORNL DAAC 2017). Only pixels which passed quality control at QC 0/1 level were included for analysis. Cloud contaminated pixels (2) or pixels contaminated for another reason (3) were omitted. Because we are performing climate trend analysis, we chose 8 day composite LST rather than the original daily LST to minimise missing data. Cloud information (number of clear days in each composite) was an important supplementary variable.

The temperature difference for each 8 day composite between LST and equivalent air temperatures (T_x and T_n) for each station was calculated over the 15 year period (2002-2017). This was called ΔT (LST minus T_{air}). Station coordinates were checked on Google Earth to ensure that the LST for the relevant pixel was extracted. We compare Aqua at 1330 LST with T_x, and Aqua at 0130 LST with T_n, since these times were the most appropriate. Although we could in theory calculate mean T_x and T_n just for the cloud-free days included in the composite to reduce the difference, for reasonable climate trend analysis we wish to derive mean T_x/T_n over the whole 8 days, so we used the latter as our predictand and ignored any potential mismatch in days when calculating ΔT.

We developed a model to predict ΔT. The main predictors were a) diurnal temperature range in Aqua LST (daytime LST minus previous night LST), b) morning heating rate between 1030 and 1330 LST (daytime model) or night time cooling rate between 2230 and 0130 LST (night-time model), c) a solar variable representing season (proxy for solar elevation), highest at the winter solstice and lowest at the summer solstice, d) frequency of cloud free days in composite, and e) frequency of cloud free nights in composite. Both d and e were included in both models of daytime and night time ΔT. These predictors were selected because response of the surface to solar radiation is suspected to be the main control of the amount of surface heating relative to the lower atmosphere (i.e. ΔT). This is determined by both the sensitivity of the surface (represented by predictors a and b), and the amount of solar input (represented by predictors c, d and e).

The model predicting ΔT (at day and at night) was run using data for each octtad (8 day period) between 2002 and 2017 (n=726). Models were optimised for each location by backward stepwise regression, retaining variables only if they were significant at $p<0.1$. Once models had been derived, they were then applied to convert LST to T_{air}, using the specific model for each station. Thus we had 87 models each for T_x and T_n. Trends in raw air temperatures, raw LST and corrected LST were then

examined at the 87 stations. 2002-2017 was the common period of analysis, limited by the LST data, so of necessity we compare trends for this period alone.

To apply the model to examine warming trends in mountain ranges without any in situ weather stations, we chose three sub-areas (Qilian, NyenchenTanglha and Himalaya) with considerable elevation range, shown by boxes in Figure 1. For each area we fine-tuned the model based on the nearest weather station. We then examined the spatial pattern of temperature trends for raw and corrected LST and their elevational dependency. Trend magnitudes were measured by the gradient of the ordinary least squares regression line (converted to °C/decade), significant at $p<0.05$.

4. Results

4.1 Temporal patterns of ΔT

The behaviour of ΔT is as expected from a basic understanding of atmospheric physics. During the day the surface LST is usually higher than T_x, and at night surface LST is usually lower than T_n. This is despite the temporal mismatch which means that the LST overpasses potentially underestimate diurnal extremes. The surface usually shows a much more extreme diurnal cycle in temperature than the free atmosphere at 2 m, particularly at high elevations in the Tibetan plateau where moisture is limiting and there is a dominance of sensible heating over latent heating for much of the year. The influence of seasonality is clearly seen in the graphs of ΔT for individual stations (Figure 2 , shown as red dots on Figure 1). During the day, the heating is enhanced when the incoming solar input is stronger (i.e. spring and summer) but also reduced at some sites in July and August due to the impact of the Tibetan Plateau monsoon which increases humidity and cloud cover, and will increase latent heating. Sites in the southern and eastern plateau (e.g. Dingri and Baingoin) are more strongly influenced by the monsoon than those in the north and west (e.g. Mangya). Bomi (Figure 2d) is in one of the wettest parts of the plateau with lush vegetation and frequent cloud cover, and the reduced ΔT in summer is clear.

Similar figures for night time ΔT (Figure 3) show smaller differences at most sites, agreeing with many other past studies [Maeda and Hurskainen, 2014; Pepin et al., 2016]. The exception is at Bomi (Figure 3d) where large negative values occur throughout the year, but particularly in summer which is a cloudy time. This is likely due to the erroneous identification of cloud covered pixels as surface temperature which is known to be a problem in more cloudy regions at night [Zhang et al., 2016], and can cause differences as big as -20 °C. This is clearly unrealistic at night when there is limited or no solar forcing. Bomi is an exceptional site and this problem was not widespread, but needs to be kept in mind when examining model performance (see subsequent section). A similar problem may have occurred at Dingri (Figure 3 c) on some summer nights, but the issue is much less frequent.

Graphs showing the mean number of cloud free days or night for each octtad are shown in Figure 4, and clearly illustrate the influence of the monsoon in increasing cloud cover during summer at stations in the south and east of the plateau, and the higher cloud rates during the day compared with the night (a result of diurnal convection). Diurnal contrasts are particularly marked at Mangya and Dingri during spring.

4.2 Modelling of ΔT

We developed stepwise regression models to predict both daytime and night time ΔT. Since daytime ΔT is more variable (and challenging to predict) we concentrate our discussion on model results for daytime. The most useful predictor is the raw diurnal temperature range in Aqua LST. In arid regimes with a strong diurnal temperature cycle, most solar energy goes into sensible heating and daytime

ΔT is high. Using diurnal LST range in the Aqua data as a single predictor of ΔT, mean model r^2 is around 0.7. However when the other four factors listed in the methods section are also included mean model r^2 rises to 0.79 (Figure 5a). There are also consistent spatial gradients in model performance which improves with latitude (Figure 5b), but deteriorates with longitude (Figure 5c) and at lower elevations (Figure 5d). The most problematic stations are in the south-east at lower elevations dominated by the South Asian summer monsoon, which increases cloudiness and precipitation.

Table 1 shows the number of times each predictor was included in the models for ΔT daytime and night time and the signs of the coefficients. Only significant +/- coefficients ($p<0.05$) are included. The diurnal range is the most important predictor in the daytime models (left hand side of the table), being included in all 87 models, and its coefficient is always positive. Morning heating rate is an important additional predictor in nearly all cases (again positive). In both cases more rapid morning heating and a greater diurnal temperature range proceed a larger ΔT. The other predictors are also fairly consistent, the solar term being negative (meaning larger differences in summer when radiation input is stronger). Interestingly the cloud free days predictor has a negative relationship with daytime ΔT once the other variables are included due to interactions between variables. As perhaps expected, night time cloud is a more reticent predictor for the daytime model and its exact influence depends on station location.

Night time predictors are shown in the right hand side of the table. The night time cooling rate is the strongest and most consistent predictor, always having a positive effect. It is difficult to interpret exact signs because of the multicollinearity effect between predictors (particularly the first two). It is more important that predictors are a) included in the model and b) have consistent sign, showing that the models are robust and do not vary much from station to station.

Station models were then used to correct LST, calculated as original LST minus the modelled ΔT (LST –(ΔT)). The corrected LST should be a much better approximation of T_x or T_n than the original LST. To test this we regressed corrected LST against T_x. An example is shown in Figure 6 for station 51886 (Mangya) in the north of the plateau where the model works extremely well. Although the original LST (Aqua 1330) shows a strong correlation with T_x (Figure 6a: r = 0.968), the instantaneous differences are large, often over 20°C. A high correlation alone therefore does not mean a good prediction. Once corrected by subtracting modelled ΔT (Figure 6b), there is much stronger correspondence between the two measurements (r=0.987) and no systematic bias (RMSE =1.69°C). The original uncorrected LST at night (Figure 6c: r=0.985) shows a much smaller but consistent bias (LST colder than T_n) which is also successfully minimised using the model (r=0.990, RMSE =1.44°C) (Figure 6d).

Results at most stations are extremely encouraging with corrected daytime LST very similar to observed T_x and any systematic bias removed. Model r^2 between corrected LST and T_x averages around 0.9 across all stations, but 40 show stronger correlations, and 25 stations (including Mangya shown in Fig. 6), above 0.95. Corrected night time LST was even more similar to observed T_n, with r2 averaging 0.925, and most stations (66) above 0.9.

The exception to good model performance occurs in the south-eastern monsoonal region. Most ill-fitting stations are in incised valleys within this region. A topographical analysis comparing model r^2 with slope aspect and exposure (details not shown) identified a reasonable correlation between model performance and topographic convexity around the station at 10 km scale. Stations which were in concavities (bowls or valley locations) showed worse performance, particularly at night. Particularly poor stations for T_x included Pali (r2=0.697) and Muli (r2=0.715) and for T_n included Muli

(r2=0.684), Chayu (r2=0.660) and Bomi (r2=0.685). The meta-correlation between overall topographic exposure index (representing concavity) and model r^2 for T_n models was 0.536. This suggests that microclimate factors could control more incised river valleys, particularly at night. Sporadic temperature inversions could be responsible for influencing T_n and LST in contrasting ways which would in part explain weaker model performance here, but further work is required to confirm this. Poorly performing stations are also in the area where the monsoonal influence is strong (mean annual precipitation>1000 mm, nearly all in summer). Thus another reason for bad model fit is probably deficiencies in the original LST data, particularly at night due to the influence of unidentified cloud, erroneously measured as cloud-free and included in the 8 day composite LST. This is known to be a common issue [Zhang et al., 2016] and LST can underestimate T_n by as much as 20°C during the warmer part of the year (i.e. the summer monsoon season). Model correction will not remove this error. Further work therefore needs to concentrate on removing the erroneous cloud rather than fine-tuning the model which is only as good as the data which goes into it.

Over most of the plateau, especially northern and western regions, where there is a current lack of weather stations, the model performs well, and can reasonably be used to convert LST into a proxy for T_x or T_n. In most cases the RMSE between corrected LST and T_x/T_n is around 1.5 to 2.5°C.

5. Trend analysis: mean temperature trends over the satellite period (2002-2017)

We performed trend analysis on a) the original T_x/T_n data, b) the original (uncorrected) LST and c) corrected LST (Table 2). The broad patterns are

a) The mean trend across all 87 stations is positive (warming) for all groups.
b) T_{air} trends are much more consistent than raw LST trends.
c) Both T_x and T_n trends average slightly less than 0.1°C/decade. However the raw LST trends are much weaker during the day (+0.02°C/decade) but much stronger during the night (+0.18°C/decade).
d) Corrected LST trends more closely approach T_{air} trends but magnitudes are slightly steeper, (+0.11°C/decade –day and +0.14°C/decade –night). The extreme differences in trend magnitudes between day and night in the raw LST data are eradicated when LST is corrected.
e) Very few stations show significant negative trends, apart from in the raw uncorrected daytime LST data. Warming is statistically significant ($p<0.05$) at around 50% of stations (sometimes more) depending on data source used.

Spatial patterns of trend magnitudes (2002-2017) are shown in Figures 7 (T_x) and 8 (T_n). The minimum temperature trends are more consistently positive in all 3 cases, and tend to be stronger in the north-east part of the plateau. Maximum temperature trends are more variable in sign and there are quite a lot of negative trends in the original LST data (Figure 7 b) but these are removed when the LST is corrected (Figure 7 c). In general, corrected LST trends (panel c) are much more like the T_{air} trends (panel a) on average than is the original LST data (panel b), although some differences in the more detailed spatial patterns remain.

6. Application of models to correct LST trends for high elevation mountain ranges with no in situ weather stations

We chose three mountain ranges (boxes on Figure 1) which have a wide range of elevation and an adjacent (or relatively nearby) in situ weather station with strong model performance (r^2 >0.88) (Figure 9). We extracted MODIS LST for these locations as in Table 3a and corrected it using the model developed for the nearest station (r^2 in the final columns). Coefficients for the models are

listed in Table 3b. We then examined trend magnitudes, and their elevational profile, for corrected LST. Qilian mountains (Figure 9a) have a relatively low mean elevation, but range from below 2000 m to over 5700 m and have a dry continental climate. The Himalaya sub-region has the largest elevation range from just below 3000 m on the southern slopes of the Himalaya to 8729 m on Mt Everest (Figure 9b). The NyenchenTanglha mountains on the central plateau have the highest mean elevation at over 5000 m and rise to slightly above 7000 m (Figure 9c).

Elevation profiles of corrected LST trends are shown for day/night in Figures 10 and 11 for the 3 mountain regions. In general, corrected LST trends are less extreme than the original LST trends (supplementary materials: Figures S1 and S2). In the Nyenchen Tanglha region (bottom right) pixels corresponding to Nam Tso (Figure 9c) which covered around 18% of the study area (4724 m) have been removed. Much smaller lakes, for example Hala Lake (4076 m) in Qilian Central, most of which is not in the region, are included in the results.

The Qilian mountains (top left) show little elevation dependency with relatively uniform warming (<0.5°C/decade) from 2000 m up to 6000 m, although there is increased variance at higher elevations. Warming is almost universally present at all elevations. A band of enhanced warming is present in the Nyenchen Tanglha mountain range (bottom right) around 5000 m and this is strongest in the day. At night there is a general increase in warming rates up to around 6000 m in Nyenchen Tanglha. Finally, the Himalaya region (bottom left) is interesting in that no strong elevational increase in warming rates is seen at the highest elevations. Some extreme cooling trends (<-1°C/decade) recorded at high elevations in the Himalaya (17 pixels) have been omitted to avoid skewing the horizontal axis. Nevertheless, there is absolute cooling widely recorded above 6000 m, both by day and night. The correction has enhanced this pattern, which was also present in the raw data but to a lesser extent and only at night (supplementary materials). The reasons for the contrasting patterns in the three regions need further research. Very generally the correction process removes some of the variability in raw LST trends and makes the contrasts between elevations more subdued. This is reassuring since it is suggesting that the model corrects for possible local factors (solar heating, aspect, land cover) which can influence raw LST in a few pixels giving unusual trends.

7. Discussion

The models are successful at reducing the consistent bias in the LST measurements in comparison with T_{air} (e.g. Figure 6). The exception is in the south and east of the plateau where cloud cover is much more frequent [Zhang et al., 2016] and there is a particular problem of undetected cloud in the night time observations which produces LST values >20°C lower than T_{air}. Where the model does not work it is suspected that data limitations are responsible. The northern and western parts of the plateau where it is dry, and sensible heat is the main heat flux, show a strong relationship between the diurnal cycle of radiation and the T_{air}/LST contrast, the basis of the model. Frequent cloud, strong winds, and vegetation (latent heat flux) all complicate any relationship and potentially decrease the effectiveness of a simple model primarily based on solar (and cloud) terms. On the Tibetan plateau, forests are rare, and in the vast majority of locations (including weather stations used to develop the model) there is very little vegetation, usually open scrub. Thus sensible heat flux typically dominates in most locations.

An important finding is that elevation dependency in the three mountain ranges shows contrasting patterns. Qilian Central shows no strong elevation-dependency. This maybe because the study area (Figure 9b) is made up of multiple mountain ranges separated by mountain basins which will be prone to distinct microclimates. There is also relatively little permanent snow. In contrast, Enhanced

warming is shown in a belt around 5000-5500 m in Nyenchen Tanglha. This is the zone around the current permanent snowline. Enhanced loss of snow and ice in this zone would cause positive feedback as albedo decreases [Pepin and Lundquist, 2008; Rangwala et al., 2010; Guo et al., 2016]. The enhanced warming is particularly prominent in the day and this increases the likelihood that snowline retreat is at least partly responsible for this pattern. The increased sensitivity in this band at night is somewhat reduced with EDW continuing up to around 6500 m. The Himalaya region is the only one where there is extensive land well-above snowline. Enhanced warming is not observed at extreme high elevations above 6000 m. Indeed a reversal and even absolute cooling trend is seen in the LST data (both raw and corrected) above 6000 m and especially around 7000-7500 m. Thus recent EDW may not have occurred at the highest levels or at the very least may stabilise at the very highest elevations. This has been suggested by other studies on the plateau based on satellite observations [Qin et al., 2009] and through modelling [Guo et al., 2016, Gao et al. 2018]. The latter study uses WRF simulations and projects future warming rates under RCP4.5/8.5 to peak around 5000 m and slowly decrease above this. Despite agreement with these more recent studies, uncertainty in our results at these ultra-high elevations is large due to a) few pixels at this elevation (i.e. a small sample size); and b) high frequencies of cloud cover.

Furthermore, the statistical models are based on weather stations below snowline and with limited vegetation. Most are in urban compounds or on dry grassland. Thus they may not work well on snow and ice (common above 5000 m) and in forested regions (SE plateau) where the latent heat flux may be a major component of the energy partitioning, and a stronger control of the difference between LST and T_{air} [Zhang et al., 2018b]. The effect of snow cover on ΔT was examined through including snow cover presence/absence as a predictor in the regression models at each CMA station, but it had very limited influence on model success and was dropped (results not shown). This was probably a result of limited snow cover (<10% of days) at most stations (3000-4000 m). To examine the effect of snow and ice at higher elevations we validated the model in the Nyenchen Tanglha region on the Zhadang Glacier (5800 m) using air temperature data from 2012 (Figure 12). In panels a and b (top row), raw and corrected LST from the pixel containing the weather station is compared with measured T_{air} from the glacier weather station. The bottom panels show mean bias (LST minus T_{air}). Since the AWS is near the intersection of 4 pixels, the mean LST of the four surrounding pixels is used as well as the station pixel.

The validation is encouraging, with mean corrected LST (triangles) much closer to T_{air} measured at the Zhadang station (diamonds) than the original data (circles) (Figures 12 a/b). Mean bias is cut from +5.40°C (raw LST) to +2.07°C (corrected LST) in the daytime, and from -3.80°C (raw LST) to -1.45°C (corrected LST) at night (panels c and d). If the mean LST from the surrounding 4 pixels is used instead of the station pixel it further reduces bias, especially in the daytime where RMSE drops to +1.21°C (Figure 12 c). It might be thought that the model which is based on rock and grass/scrub would overcompensate on snow and ice, producing a corrected LST which was much too low during the day. This is not the case apart from in April and May (when there is a combination of intense sunlight and snow), and differences with T_{air} are relatively small after correction throughout most of the year.

An additional problem is that some LST trends (whether raw or uncorrected) are based on relatively few observations because of frequent cloud cover. They represent clear sky conditions which only occur a small proportion of the time. We can represent the uncertainty by calculating mean cloud frequency for each pixel, which gives a level of confidence for trend profiles shown in Figures 10 and 11. Figure 13 shows elevation profiles of cloud free frequency for the four areas. Daytime cloud (open boxes) is usually more frequent than night time cloud (shaded boxes), and above a certain

elevation, cloud often becomes more frequent. At night the transition from cloud free to cloud-covered is often rapid, suggestive of a clearly identifiable cloud base, whereas in the day the transition is more gradual as convective cloud is typically patchy and forms at various levels in the atmosphere. The critical elevation above which cloud contamination becomes a severe issue appears to be around 4500 m in Qilian mountains and 5500-6000 m in Nyenchen Tanglha. This is above the upper limit of the enhanced daytime warming identified earlier in the latter mountain range (5000-5500 m), increasing confidence that this enhancement is reliable. In contrast, the absolute cooling recorded in the Himalaya is based on LST from relatively small amounts of data, mean daytime clear-sky frequencies dropping to around 1 day in 8 (12.5%) above 6500 m.

Because of possible limitations, we have not extended our approach to determine an EDW profile for the whole Tibetan plateau in this paper. First, if a representative profile were to be derived, this would require agreement on the extent of the plateau or "representative area". Second, it would also require the development of a region-wide model rather than solely combining 87 different station-based models. Of necessity, the fine-tuning of the model to specific mountain ranges, where it can be used to quantify a spatial trend pattern dominated by elevation, would be compromised. Third, to improve confidence in the south-eastern region, further work is required to consider the role of cloud feedback processes on EDW. An additional obstacle is the lack of reliable LST data [Zhang et al. 2016], rather than just limitations in our radiative-based model.

Finally, we must be careful of over-interpreting trends based on a fairly short period. The early 21st century was in part influenced by the hiatus in climate warming [Knight et al., 2009], although it is debatable whether warming slowed on the Tibetan Plateau [Yan and Liu, 2014], and recent work has suggested that the plateau was not influenced [Duan and Xiao 2015]. Irrespective of this issue, trends derived over 16 years may not represent a longer time period. As LST records increase in length, they will become more valuable for climate trend analysis.

8. Summary

We developed individual station-based models at 87 CMA stations to correct raw LST to make it more representative of air temperature over the Tibetan plateau. These models removed 80-90% of the difference between LST and T_{air} for the equivalent pixel. Models were less successful for stations in the south-eastern plateau where monsoonal influence is strong, in part due to deficiencies in the LST data. We analysed elevational profiles in trend magnitudes (2002-2017) for raw and corrected LST for 3 main mountain ranges across the northern, central and south-western Tibetan plateau, where the model was successful (r^2>0.88). Results show a marked peak in warming rates around 5000-5500 m in Nyenchen Tanglha, most noticeable in the daytime data. Snow cover decline (in turn influencing albedo feedback) is suggested to be the most obvious reason for this enhanced warming. The Qilian mountains showed limited elevation dependency. The Himalaya region saw warming rates decrease in both raw and corrected data above 6000 m, but this is the only region which extends to the very highest elevations. The cooling observed at the highest elevations is rather uncertain because of the small number of pixels (statistical uncertainty) coupled with high frequencies of cloud cover. Together these results suggest that EDW profiles depend on the mountain range examined, and enhancement of warming is probable up to and including current receding snowline regions, but that there may be a stabilisation in recent warming rates at the very highest elevations.

Acknowledgements

Nick Pepin was supported by a PIFI scholarship provided by the Chinese Academy of Sciences and hosted by the Institute of Tibetan Plateau Research. This study was supported by the Strategic Priority Research Program of the Chinese Academy of Sciences (XDA20060202). The authors thank the Nam Co Station for Multisphere Observation and Research for providing ground measurements of air temperature data (Zhadang Glacier). In addition, the authors are grateful to the Chinese Meteorology Administration (http://data.cma.cn/data/cdcdetail/dataCode/SURF_CLI_CHN_MUL_DAY_V3.0.html) for providing air temperature data. The raw LST data is available from https://modis.ornl.gov/cgi-bin/MODIS/global/subset.pl. The corrected LST data is available from the University of Portsmouth data repository at https://doi.org/10.17029/be8cae2c-e527-4f0c-b557-ad3c3d97823e.

References

Benali, A., Carvalho, A.C., Nunes, J.P,, Carvalhais, N., and Santos, A. (2012), Estimating air surface temperature in Portugal using MODIS LST data, *Remote Sensing of Environment,* 124, 108-121.

Bosilovich, M.G. (2006), A comparison of MODIS land surface temperature with in situ observations, *Geophys. Res. Lett.*, 33, L20112, doi:10.1029/2006GL027519.

Collins, M. et al. (2013) Long-term Climate Change: Projections, Commitments and Irreversibility. In: Climate Change 2013: The Physical Science Basis. Contribution of Working Group I to the Fifth Assessment Report of the Intergovernmental Panel on Climate Change [Stocker, T.F. et al. (eds.)]. Cambridge University Press, Cambridge, United Kingdom and New York, NY, USA, pp. 1029–1136, doi:10.1017/CBO9781107415324.024.

Comiso, J.C., and Hall, D.K. (2014). Climate trends in the Arctic as observed from space, *Wiley Interdiscip. Rev.: Clim. Change*, 5(3), 389–409.

Deng, H., N. C. Pepin, and Y. Chen (2017), Changes of snowfall under warming in the Tibetan Plateau, J. Geophys. Res.Atmos., 122(14), 7323-7341, doi:10.1002/2017JD026524.

Duan, A., and Wu, G. (2006), Change of cloud amount and the climate warming on the Tibetan Plateau, Geophys. Res. Lett. 33, L22704.

Duan A, Xiao Z (2015) Does the climate warming hiatus exist over the Tibetan Plateau? Sci Rep 5:13711. doi: 10.1038/srep13711

Gao, Y., Chen, F., Lettenmaier, D.P., Xu, J., Xiao, L. & Li, X. (2018). Does elevation-dependent warming hold true above 5000 m elevation? Lessons from the Tibetan Plateau, npj Climate and Atmospheric Science (2018) 1:19 ; doi:10.1038/s41612-018-0030-z.

Good, E. (2015), Daily minimum and maximum surface air temperatures from geostationary satellite data, J. Geophys. Res. Atmos., 120, 2306–2324, doi:10.1002/2014JD022438.

Good, E. J. (2016), An in situ-based analysis of the relationship between land surface "skin" and screen-level air temperatures, J. Geophys. Res. Atmos., 121, 8801–8819, doi:10.1002/2016JD025318.

Guo, D. L., and H. J. Wang (2012), The significant climate warming in the northern Tibetan Plateau and its possible causes, Int. J. Climatol., 32, 1775–1781.

Guo, D., E. Yu, and H. Wang (2016), Will the Tibetan Plateau warming depend on elevation in the future?, J. Geophys. Res. Atmos., 121, 3969–3978, doi:10.1002/2016JD024871.

Knight, J., Kennedy, J., Folland, C., Harris, G., Jones, G., Palmer, M., Parker, D., Scaife, A., and Stott, P. (2009), Do global temperature trends over the last decade falsify climate predictions, Bull. Am. Meteorol. Soc, 90(8), 22-23.

Kustas, W., and Anderson, M. (2009), Advances in thermal infrared remote sensing for land surface modeling, Agricultural and Forest Meteorology, 149 (12), 2071–2081.550.

Lau, W., Kim, M., Kim, K., and Lee, W. (2010), Enhanced surface warming and accelerated snow melt in the Himalayas and Tibetan Plateau induced by absorbing aerosols, Environ. Res. Lett. 5(2), 025204.

Lawrimore, J.H., Menne, M.J., Gleason, B.E., Williams, C.N., Wuertz, D.B., Vose, R.S., and Rennie, J. (2011), An overview of the Global Historical Climatology Network monthly mean temperature data set, version 3, J. Geophys. Res., 116, D19121, doi:10.1029/2011JD016187.

Lundquist, J.D., Chickadel, C., Cristea, N., Currier, W.R., Henn, B., Keenan, E., and Dozier, J. (2018), Separating snow and forest temperatures with thermal infrared remote sensing, Remote Sensing of Environment, 209, 764-779, doi.org/10.1016/j.rse.2018.03.00.

Maeda, E.E., and Hurskainen, P. (2014), Spatiotemporal characterization of land surface temperature in Mount Kilimanjaro using satellite data, Theor. Appl. Clim., DOI:10.1007/s00704-013-1082-y.

Merchant, C.J., Matthiesen, S., Rayner, N.A., Remedios, J.J., Jones, P.D., Olesen, F., Trewin, B., Thorne, P.W., Auchmann, R., Corlett, G.K., Guillevic, P.C., and Hulley, G.C. (2013), The surface temperatures of Earth: steps towards integrated understanding of variability and change, *Geosci. Instrum. Method. Data Syst.*, 2, 305-321, doi:10.5194/gi-2-305-2013.

Mildrexler, D.J., M. Zhao, and S.W. Running (2011), A global comparison between station air temperatures and MODIS land surface temperatures reveals the cooling role of forests, J. Geophys. Res., 116, G03025, doi:10.1029/2010JG001486.

Minder, J. R., T. W. Letcher, and S. M. Skiles (2016), An evaluation of high-resolution regional climate model simulations of snow cover and albedo over the Rocky Mountains, with implications for the simulated snow-albedo feedback. *J. Geophys. Res. Atmos.*, 121, 9069–9088, https://doi.org/10.1002/2016JD024995.

Mostovoy, G.V., King, R., Reddy, K. R., and Kakani, V.G. (2005), Using MODIS LST data for high-resolution estimates of daily air temperature over Mississippi. In *Proceedings of the 3rd international workshop on the analysis of multi-temporal remote sensing images.* pp 76-80). IEEE, CD Rom

Nemani, R.R., and Running, J.W. (1989), Estimation of regional surface resistance to evapotranspiration from NDVI and thermal-IR AVHRR data, *Journal of Applied Meteorology*, 28, 276–284.

Ohmura, A. (2012), Enhanced temperature variability in high-altitude climate change, Theoretical and Applied Climatology, 110, 499-508.

ORNL DAAC. (2017), MODIS Collection 6 Land Products Global Subsetting and Visualization Tool. ORNL DAAC, Oak Ridge, Tennessee, USA. Accessed April 19, 2018. Subset obtained for MYD11A2 product at 38.4587N,99.5436E, time period: 2002-07-04 to 2018-04-07, and subset size: 5 x 5 km. https://doi.org/10.3334/ORNLDAAC/1379

Østby, T.I., Schuler, T.V., and Westermann, S. (2014) Severe cloud contamination of MODIS Land Surface Temperatures over an Arctic ice cap, Svalbard, *Remote Sensing of Environment*, 142, 95-102.

Osborn, T.J., and Jones, P.D. (2014), The CRUTEM4 land-surface air temperature data set: construction, previous versions and dissemination via Google Earth, *Earth System Science Data,* 6, 61-68, doi:10.5194/essd-6-61-2014.

Oyler, J. W., A. Ballantyne, K. Jencso, M. Sweet, and S. W. Running (2015), Creating a topoclimatic daily air temperature dataset for the conterminous United States using homogenized station data and remotely sensed land skin temperature, Int. J. Climatol., 35, 2258–2279, doi:10.1002/joc.4127.

Oyler, J. W., Dobrowski, S. Z., Holden, Z. A., and Running, S. W. (2016), Remotely sensed land skin temperature as a spatial predictor of air temperature across the conterminous United States, Journal of Applied Meteorology and Climatology, 55(7), 1441–1457. https://doi.org/10.1175/JAMC-D-15-0276.1.

Parmentier, B., B. J. A. M. McGill, W. J. Regetz, W. Jetz, R. Guralnick, M.-N. Tuanmu, and M. Schildhauer (2015), Using multi-timescale methods and satellite-derived land surface temperature for the interpolation of daily maximum air temperature in Oregon, Int. J. Climatol., 35, 3862–3878, doi:10.1002/joc.4251.

Pepin, N.C., and Lundquist, J. (2008), Temperature trends at high elevations: Patterns across the globe, Geophysical Research Letters, 35, L14701, doi:10.1029/ 2008GL034026.

Pepin, N.C., Bradley, R.S., Diaz, H. et al. (2015), Elevation-dependent warming in mountain regions of the world, Nature Climate Change, 5(5), 424-430.

Pepin, N.C., Maeda, E.E., and Williams, R. (2016), Use of remotely-sensed land surface temperature as a proxy for air temperatures at high elevations: Findings from a 5000 metre elevational transect across Kilimanjaro, *J. Geophys. Res.Atmos.,* 121(17), 9998-10015, doi: 10.1002/2016JD025497.

Pepin, N.C., Pike, G., Read, S., Williams, R. (2018). The ability of MODIS land surface temperatures to simulate cold air drainage and microclimates in complex Arctic terrain, *Int Jnl Climatology*, doi: 10.1002/joc.5854

Qin, J., K. Yang, S. Liang, and X. Guo (2009), The altitudinal dependence of recent rapid warming over the Tibetan Plateau, Clim. Change, 97(1), 321–327, doi:10.1007/s10584-009-9733-9.

Rangwala, I., J. Miller, G. Russell, and M. Xu (2010), Using a global climate model to evaluate the influences of water vapor, snow cover and atmospheric aerosol on warming in the Tibetan Plateau during the twenty-first century, Clim. Dyn., 34, 859–872.

Rangwala, I., and Miller, J.R. (2012), Climate change in mountains: a review of elevation-dependent warming and its possible causes, Clim. Chang, 114, 527–547.

Rangwala, I., E. Sinsky, and J. R. Miller, (2016), Variability in projected elevation dependent warming in boreal midlatitude winter in CMIP5 climate models and its potential drivers, *Climate Dyn.*, 46, 2115–2122, https://doi.org/10.1007/s00382-015-2692-0.

Serreze, M.C., and Francis, J.A. (2006), The Arctic amplification debate, *Climatic Change*, 76, 241–264.

Serreze, M., Barrett, A., Stroeve, J., Kindig, D., and Holland, M. (2009), The emergence of surface based Arctic amplification, *Cryosphere,* 3, 11–19.

Shamir, E., and Georgakakos, K.P. (2014), MODIS Land Surface Temperature as an index for surface air temperature for operational snowpack estimation, *Remote Sensing of Environment*, 152, 83-98.

Urban, M., Eberle, J., Hüttich, C., Schmullius, C., and Herold, M. (2013), Comparison of satellite-derived land surface temperature and air temperature from meteorological stations on the pan-Arctic Scale, *Remote Sensing*, 5(5), 2348-2367.

Vancutsem, C., Ceccato, P., Dinku, T., and Connor, S.J. (2010), Evaluation of MODIS land surface temperature data to estimate air temperature in different ecosystems over Africa, *Remote Sensing of Environment*, 114(2), 449-465.

Westermann, S., Langer, M., and Boike, J. (2012), Systematic bias of average winter-time land surface temperatures inferred from MODIS at a site on Svalbard, Norway, *Remote Sensing of Environment*, 118, 162-167.

Williamson, S.N., Hik, D.S., Gamon, J.A., Jarosch, A.H., Anslow, F.S., Clarke, G.K.C., and Rupp, T.S. (2017), Spring and summer monthly MODIS LST is inherently biased compared to air temperature in snow covered sub-Arctic mountains, Remote Sensing of Environment, 189, 14-24, https://doi.org/10.1016/j.rse.2016.11.009.

Yan, L., and Liu, X. (2014), Has Climatic Warming over the Tibetan Plateau Paused or Continued in Recent Years? Journal of Earth, Ocean and Atmospheric Sciences, 1, 13-28.

Yan, L., Z. Liu, G. Chen, J. E. Kutzbach, and X. Liu (2016), Mechanisms of elevation-dependent warming over the Tibetan Plateau in quadrupled CO2 experiments, Clim. Change, doi:10.1007/s10584-016-1599-z.

Zhang, H., Zhang, F., Ye, M., Che, T., & Zhang, G. (2016), Estimating daily air temperatures over the Tibetan Plateau by dynamically integrating MODIS LST data, Journal of Geophysical Research: Atmospheres, 121, 11,425–11,441. https://doi.org/10.1002/2016JD025154.

Zhang, H., Zhang, F., Zhang, G., He, X., and Tian, L. (2016), Evaluation of cloud effects on air temperature estimation using MODIS LST based on ground measurements over the Tibetan Plateau, *Atmospheric Chemistry and Physics,* 16(21), 13,681–13,696. https://doi.org/10.5194/acp-16-13681-2016.

Zhang, H., Zhang, F., Zhang, G., Che, T., and Yan, W. (2018a), How accurately can the air temperature lapse rate over the Tibetan Plateau be estimated from MODIS LSTs? Journal of Geophysical Research: Atmospheres, 123. https://doi. org/10.1002/2017JD028243.

Zhang, H., Zhang, F. A. N., Zhang, G., Ma, Y., Yang, K. U. N., and Ye, M. (2018b), Daily air temperature estimation on glacier surfaces in the Tibetan Plateau using MODIS LST data. Journal of Glaciology, 64(243), 132–147. https://doi.org/10.1017/jog.2018.6.

Tables

Table 1: Number of times each predictor is included in the 87 regression models predicting ΔT, frequency of the sign of each predictor (+/-), and mean predictor coefficient.

Predictor (Day)	n	Number +/-	Mean coefficient	Predictor (Night)	N	Number +/-	Mean coefficient
Diurnal Range	87	87/0	0.586	Diurnal Range	79	3/76	-0.130
Morning Heating	84	84/0	0.230	Night Cooling	87	87/0	0.371
Solar Term	79	6/73	-0.169	Solar Term	66	37/29	0.019
Cloud Free Days	70	2/68	-0.226	Cloud Free Days	77	77/0	0.313
Cloud Free Nights	56	37/19	0.108	Cloud Free Nights	83	83/0	0.522

Table 2. Summary of trend magnitudes (˚C/decade) for 2002-2017 for T_{air}, raw LST and corrected LST at the 87 stations across the Tibetan Plateau. Figures in brackets are significant trends ($p<0.05$).

2002-2017	Mean trend (˚C/decade)	Number +ve trends	Number –ve trends	Number insig. trends
T_x	0.093	82 (43)	5 (2)	42
T_n	0.099	79 (57)	8 (5)	25
Raw LST Day	0.024	53 (17)	34 (12)	58
Raw LST Night	0.184	84 (60)	3 (0)	27
Corrected LST T_x*	0.111	82 (30)	5 (0)	57
Corrected LST T_n*	0.136	83 (50)	4 (0)	37

*Corrected LST using ΔT model

Table 3a: Summary of MODIS data extracted for mountainous sub-areas of the Tibetan Plateau and model r2 for each location.

Range	Central Latitude	Central Long.	Area (km)	Range in Elevation (from LST Pixels)	Station Name	Station Elev	Model r2 (max)	Model r2 (min)
Qilian Central	38.809	98.419	101 * 101	1791 – 5741 m	Tuole	3367	0.964	0.980
Himalaya	28.346	86.946	101 * 101	2961-8729 m	Dingri	4300	0.894	0.959
Nyenchen Tanglha	30.617	90.800	101 * 101	4286 – 6969 m	Dangxiong	4200	0.888	0.937

Table 3b. Coefficients for the six regression models applied to convert LST to T_{air}.

Mountain Range	Diurnal Range	Heating Rate	Solar	Cloud Day	Cloud Night	Constant	Model
Qilian Central	0.5988	0.2874	-0.3439	Not included	0.1291	-3.34	Day
Himalaya	0.7353	0.0819	-0.2298	-0.1973	0.5213	-9.312	Day
Nyenchen Tanglha	0.6201	0.1866	-0.1325	-0.2604	0.1489	-5.566	Day
Qilian Central	-0.0615	0.3370	-0.0189	0.3311	0.4690	-2.734	Night
Himalaya	0.0375	0.5299	0.0795	0.2550	0.8023	-8.337	Night
Nyenchen Tanglha	-0.0658	0.4479	0.0873	0.2811	0.4529	-4.797	Night

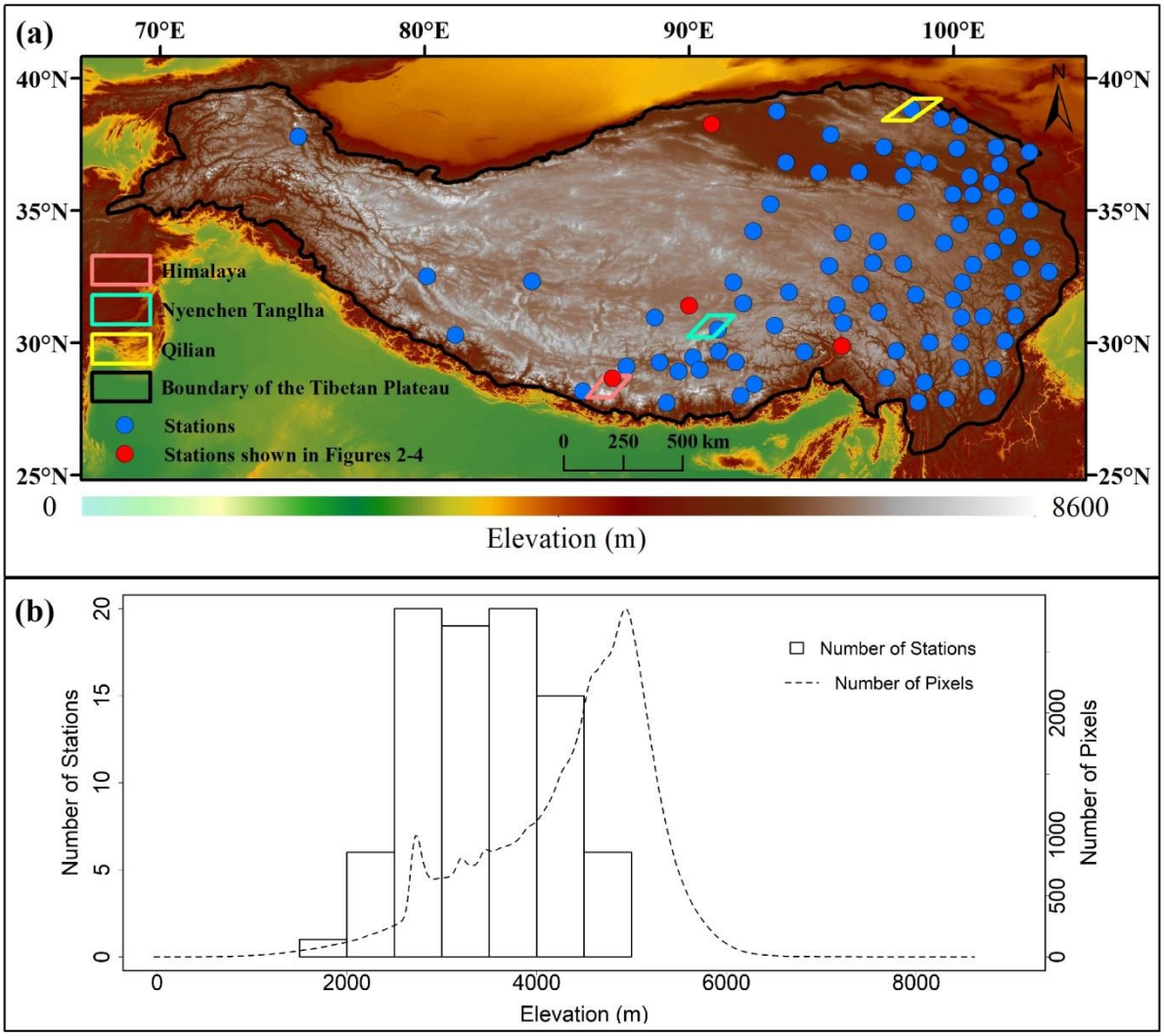

Figure 1. Map of the Tibetan Plateau showing a) the 87 CMA stations used to develop the model converting LST to T_{air}. The three mountain ranges selected for further analysis are represented by coloured boxes, stations shown in Figures 2-4 are shown in red, b) hypsometric curve of elevation over the Tibetan plateau from LST pixels (dotted line) and distribution of CMA stations (bars).

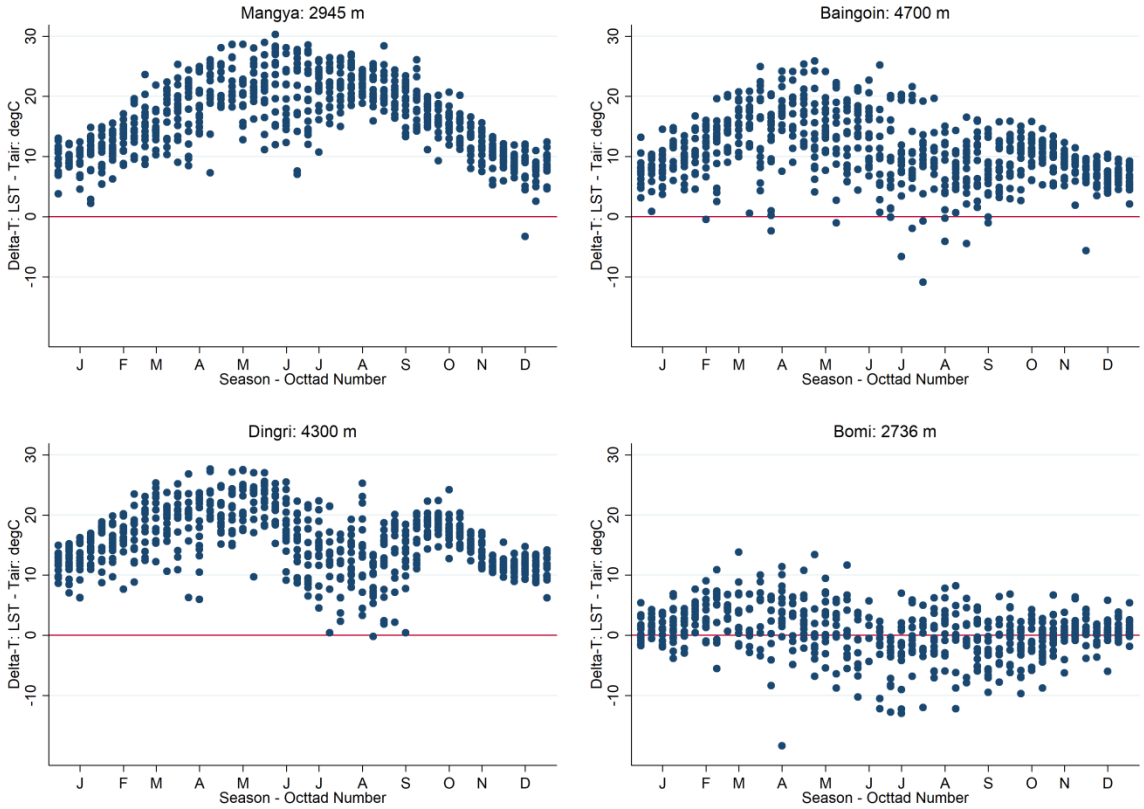

Figure 2. Seasonal patterns of daytime ΔT at a) Mangya (northern plateau), b) Baingoin (eastern Changtang), c) Dingri (Himalayan region), d) Bomi (south-eastern plateau).

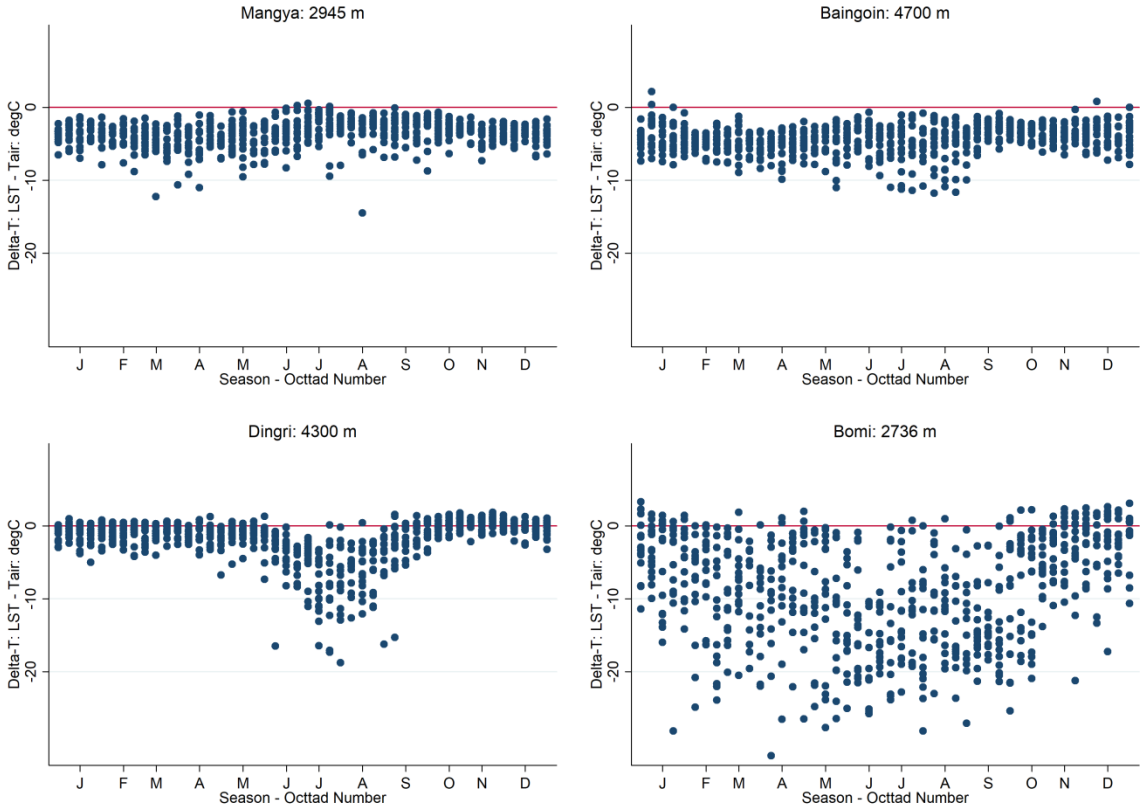

Figure 3: Same as Figure 2 but for night time ΔT.

Figure 4. Seasonal patterns in mean number of cloud free days in each composite at the four stations a) Mangya (northern plateau), b) Baingoin (eastern Changtang), c) Dingri (Himalayan region), d) Bomi (south-eastern plateau).

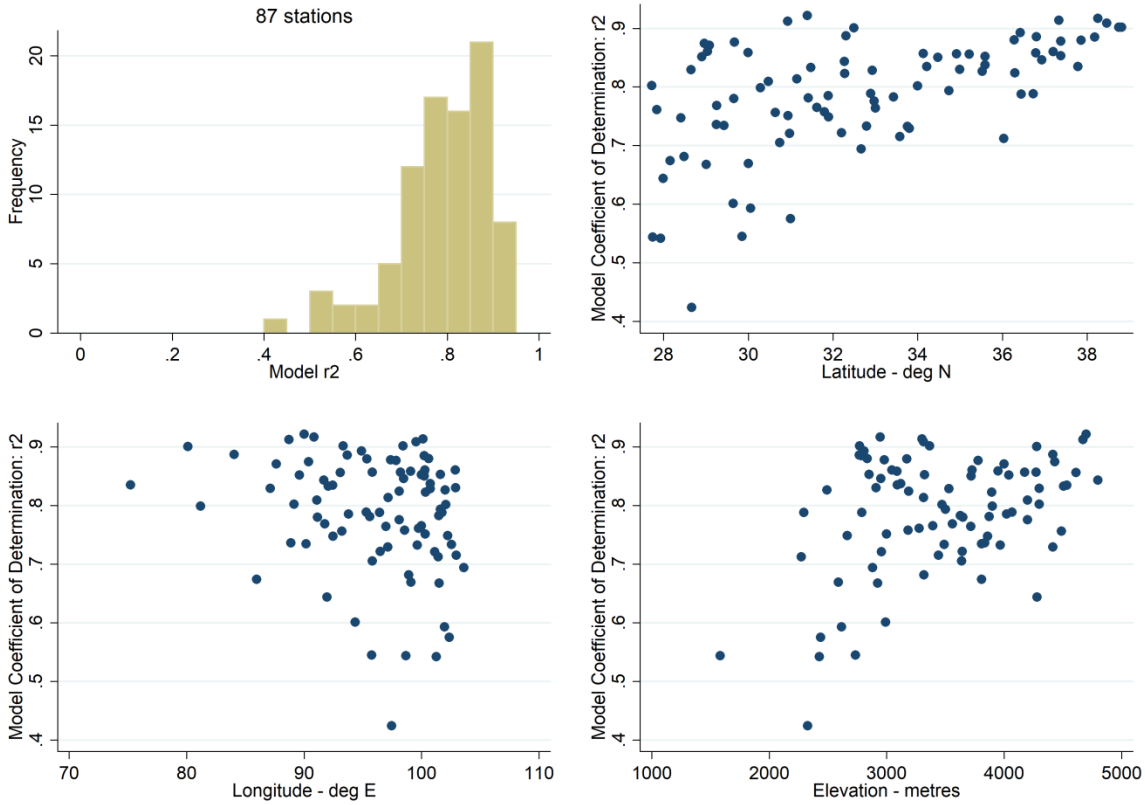

Figure 5. a) histogram of model r^2 (mean 0.79) for the full daytime model predicting ΔT. 87 models are produced, one for each in situ station. Model r^2 is also plotted against station latitude (panel b), longitude (panel c) and elevation (panel d).

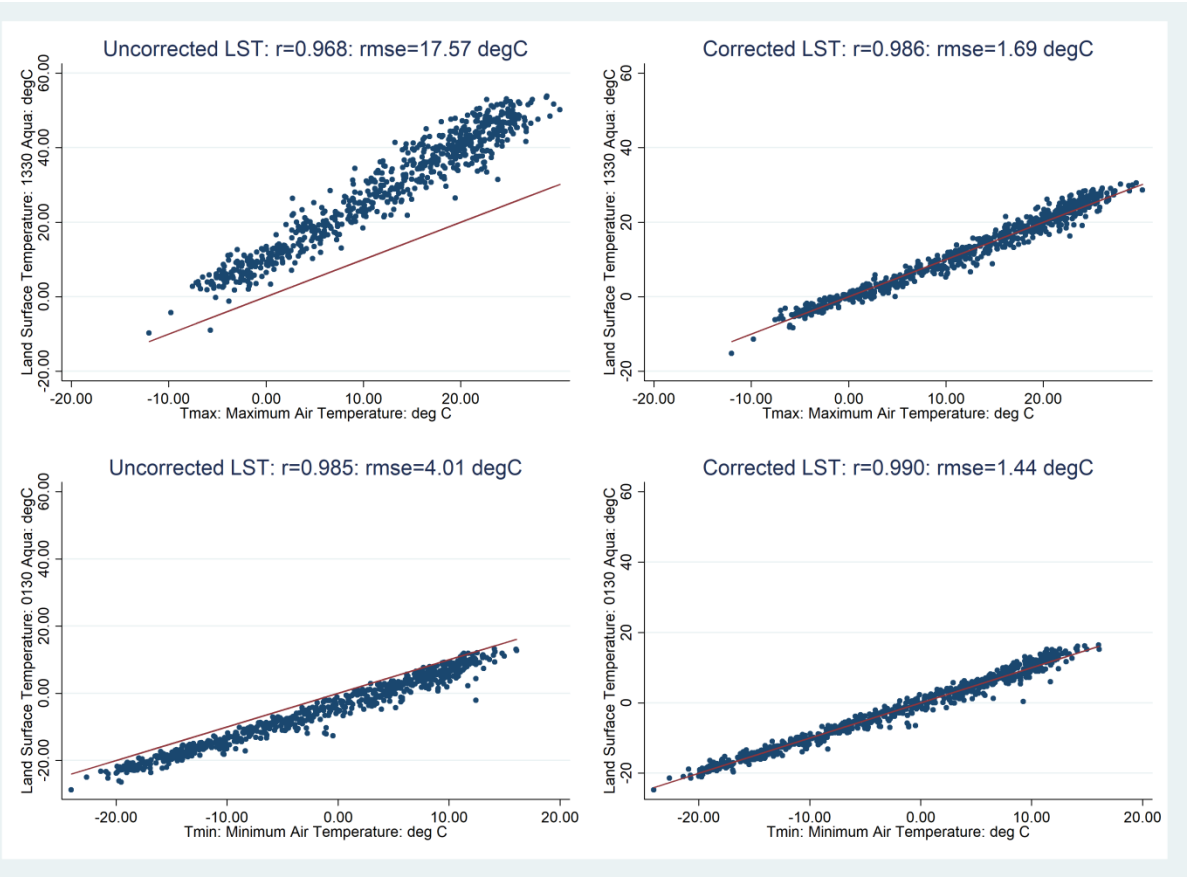

Figure 6: Example of the model correction procedure for Mangya station (51886): a) Uncorrected 1330 LST vs T_x, b) Corrected LST vs T_x, c) Uncorrected 130 LST vs T_n, d) Corrected LST vs T_n.

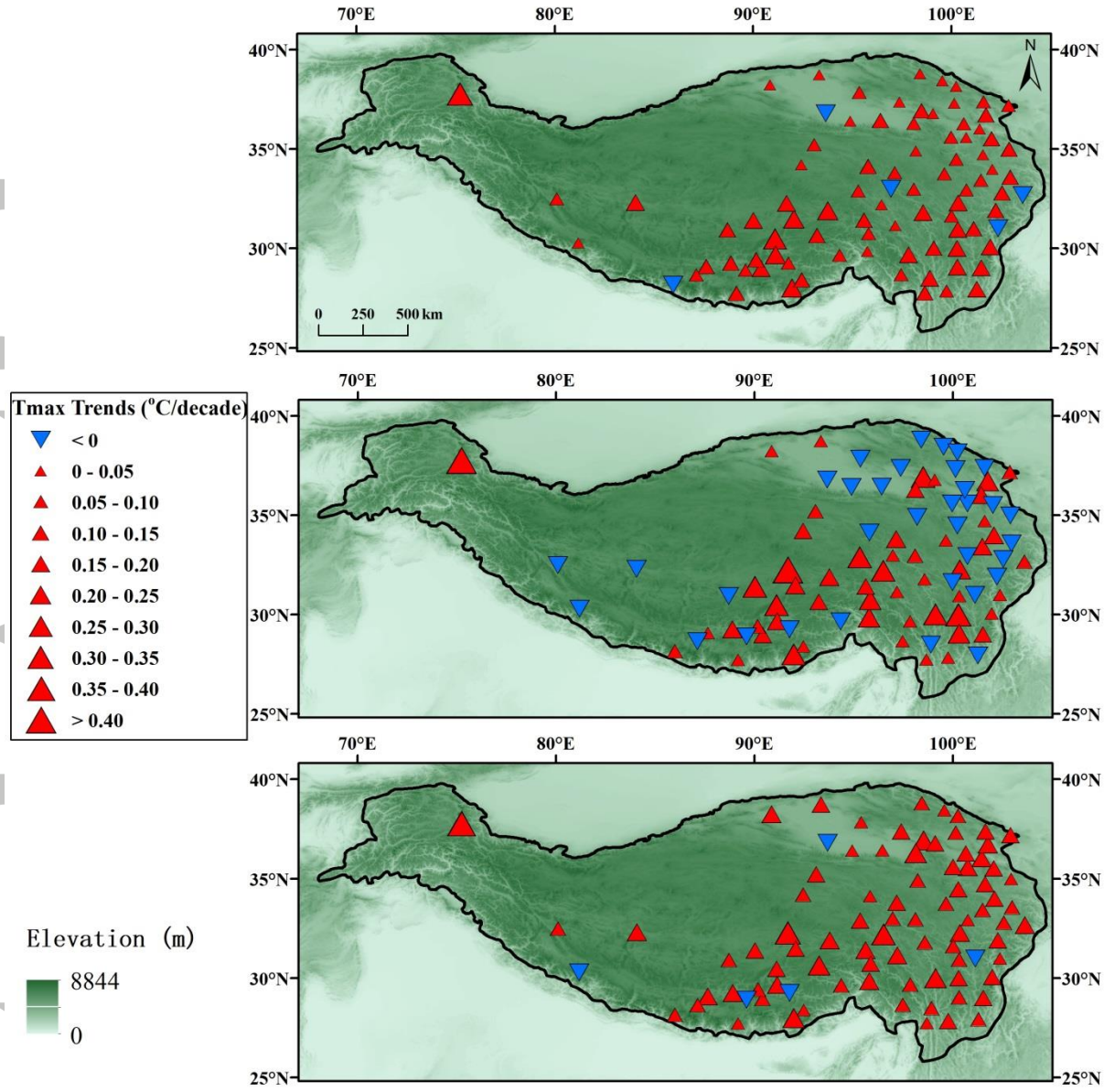

Figure 7: T_x trends (˚C/decade) for 2002-2017: top panel (raw T_x data), middle panel (raw LST data), bottom panel (corrected LST data).

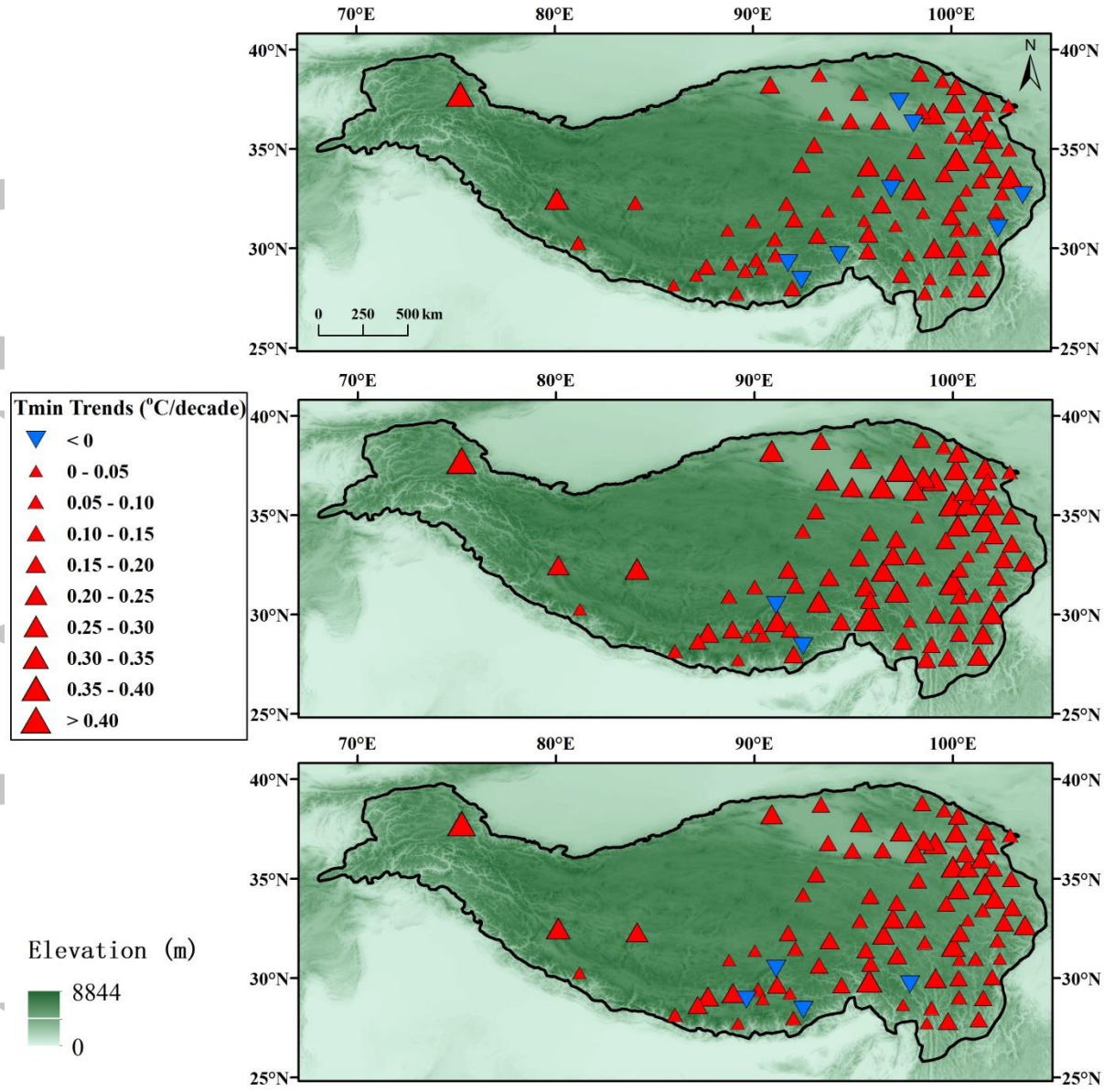

Figure 8: T_n trends (˚C/decade) for 2002-2017: top panel (raw T_n data), middle panel (raw LST data), bottom panel (corrected LST data).

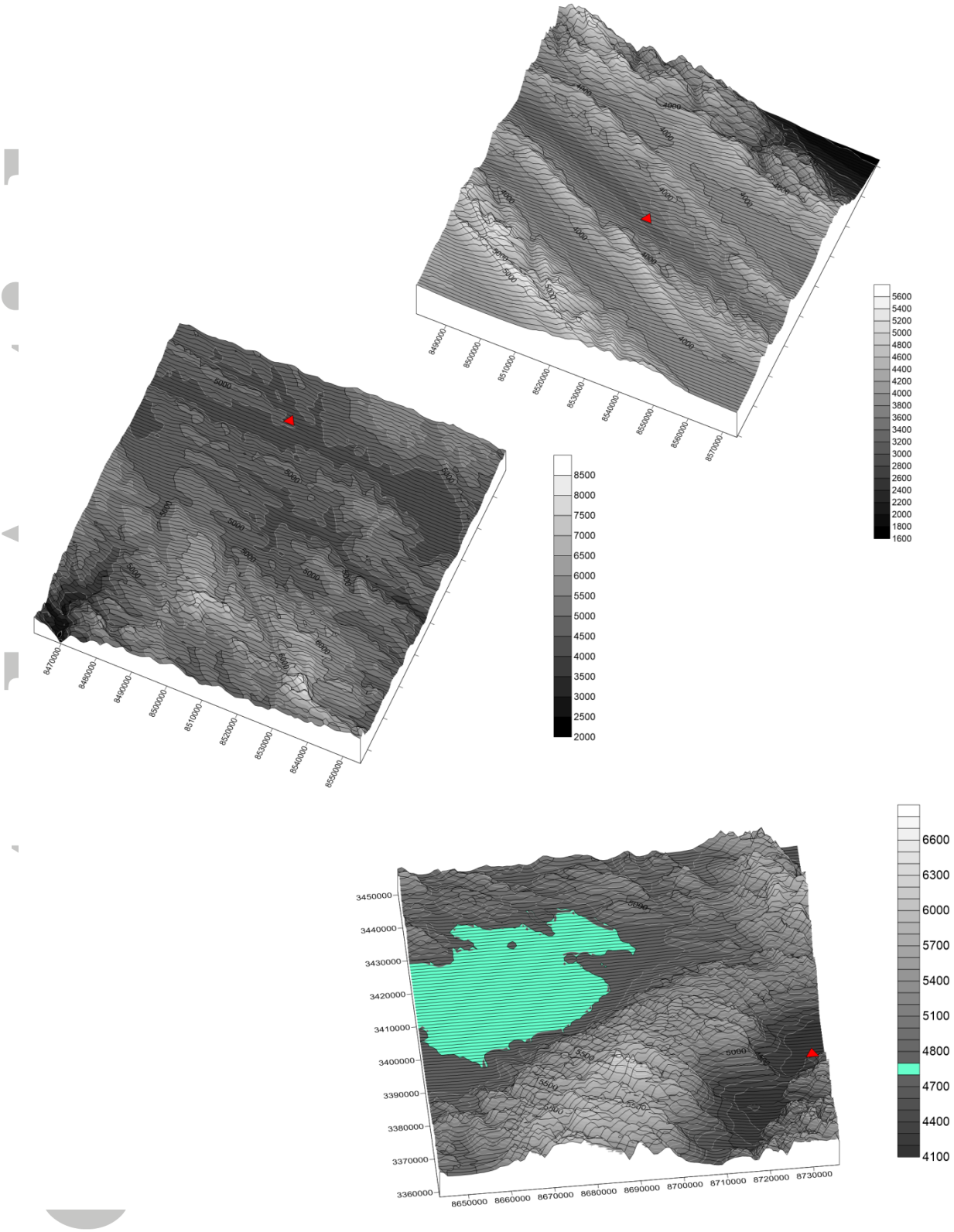

Figure 9: Maps showing detailed topography (elevation in m) of the three mountain ranges, Qilian Mountains (top), Himalaya (middle) and NyenchenTanglha (bottom). Each location is 101 km by 101 km. The large lake in the NyenchenTanglha is Nam Tso (4724 m).

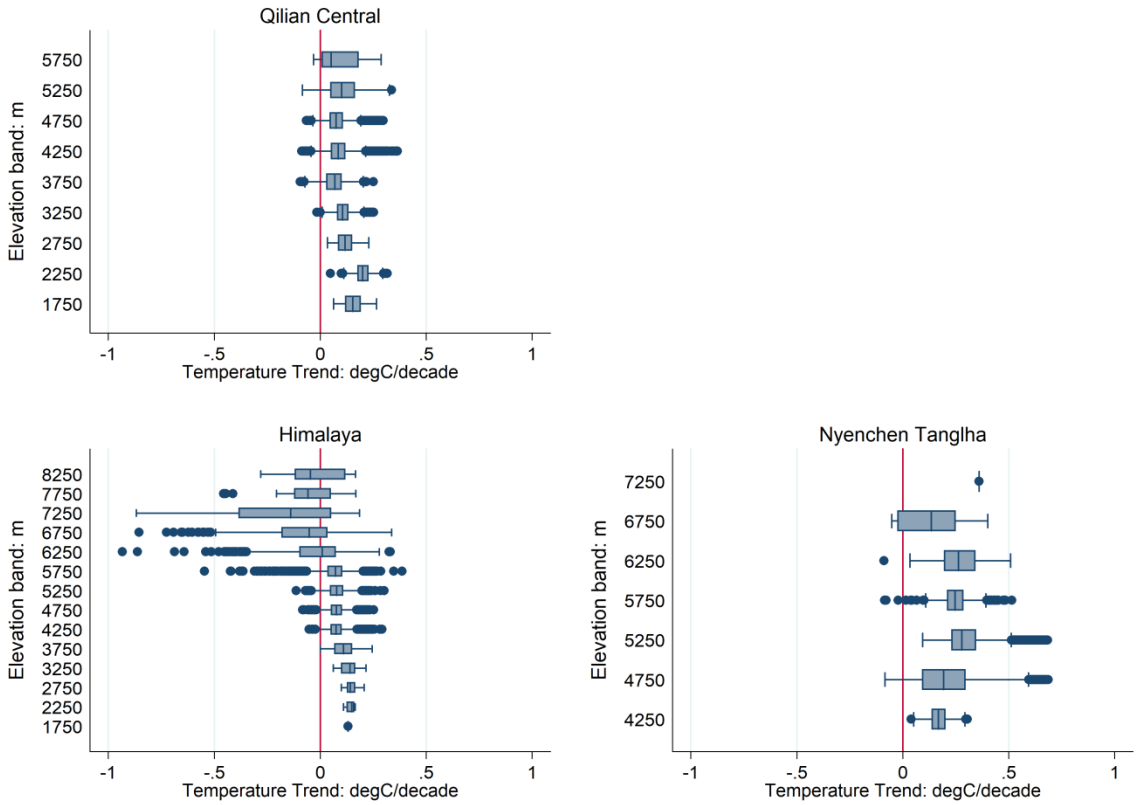

Figure 10: Daytime elevation profiles of corrected LST trends for a) Qilian Central, b) Himalaya and c) Nyenchen Tanglha. The elevation given on the y axis is the mid-elevation for each band, i.e. 2250 represents 2000-2500 m. All plots have same horizontal axis for easy comparison.

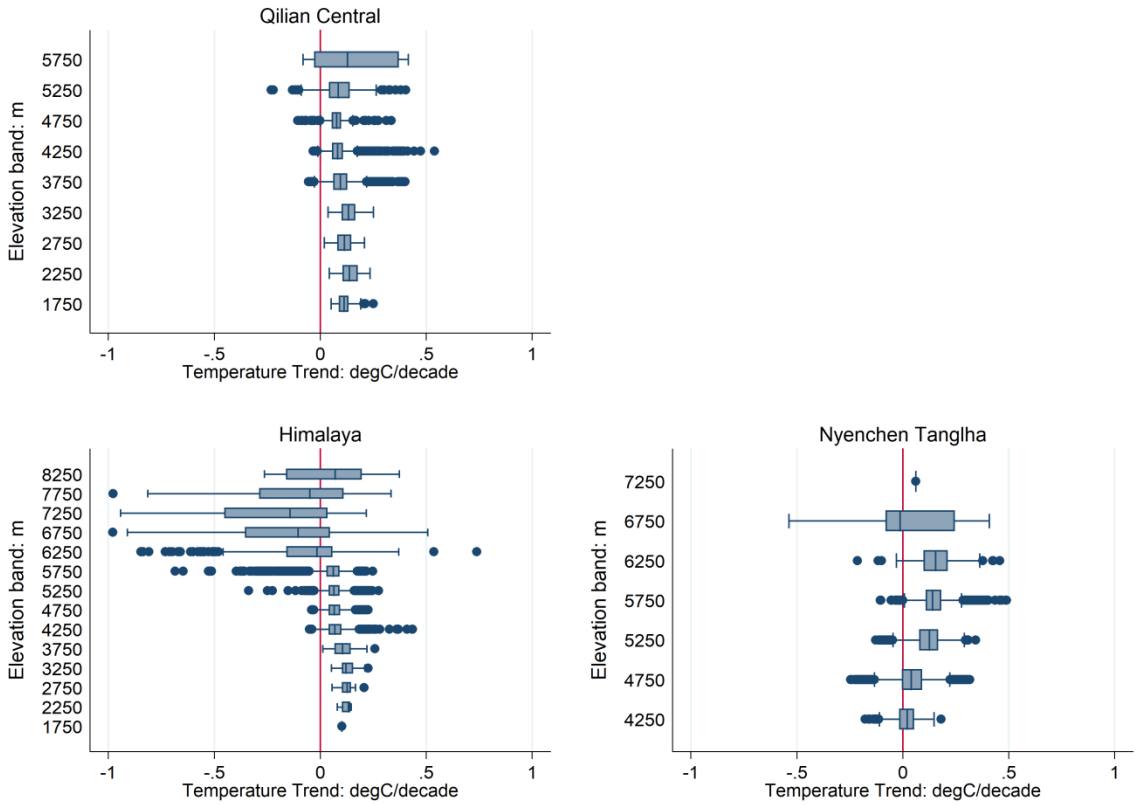

Figure 11: Same as Figure 10 for night time. Strong negative trends <-1°C/decade for 17 pixels in the Himalaya are omitted to avoid skewing the horizontal axis.

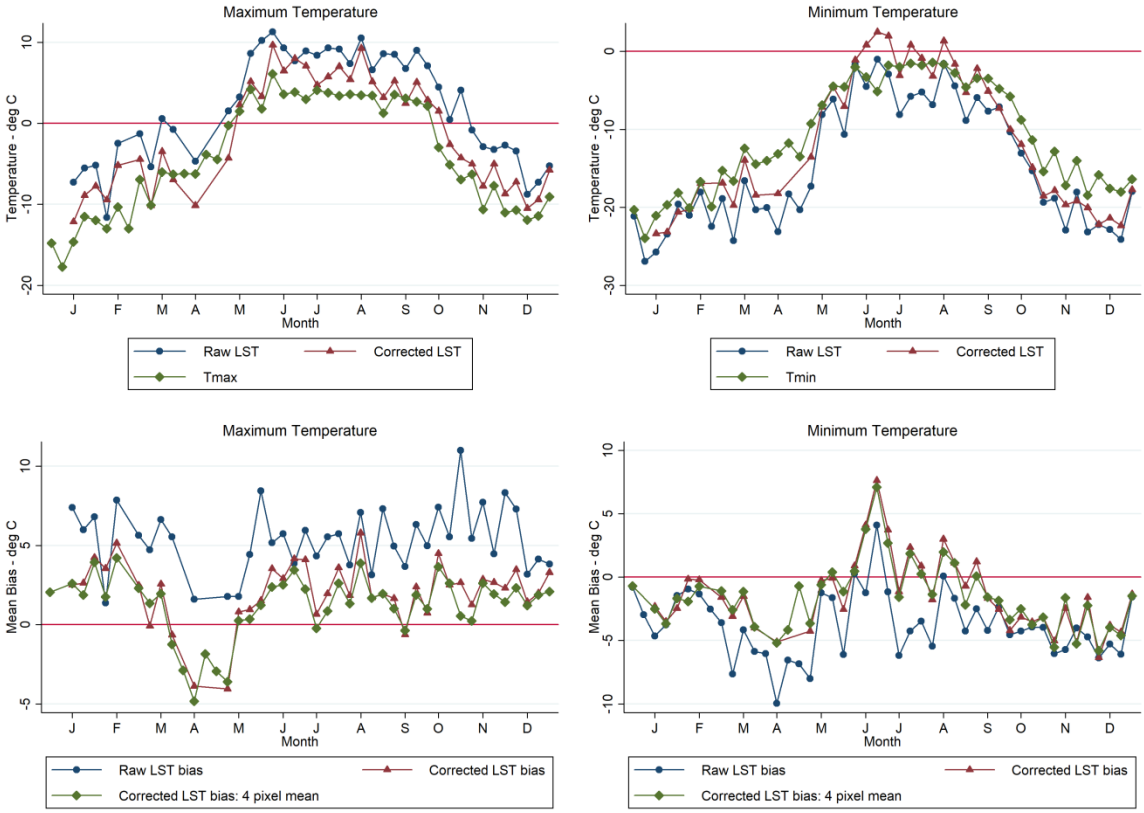

Figure 12: Validation of LST correction model using air temperatures recorded in 2012 at Zhadang glacier (5800 m) in the NyenchenTanglha mountain range. a) T_x and b) T_n are compared against raw (circles) and corrected (triangles) daytime/night time LST for the pixel in which the weather station is cited. Panels c) and d) show seasonal patterns in mean bias (LST minus T_{air}) for raw and corrected LST. Bias is based on the station pixel (triangles) and the mean of four surrounding pixels (diamonds).

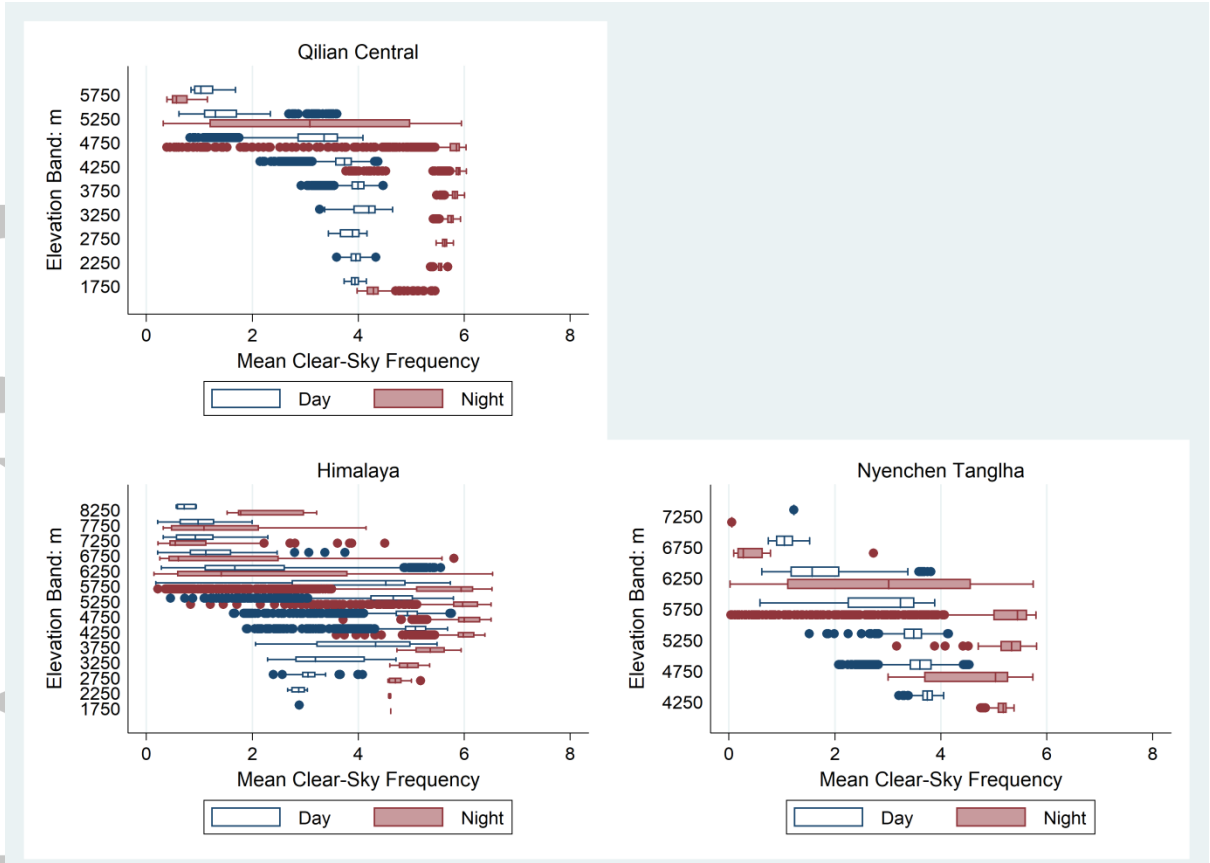

Figure 13: Vertical profiles in mean cloud free frequency in each 8 day composite, for a) Qilian Central, b) Himalaya and c) Nyenchen Tanglha. Night time (shaded boxes) and Daytime (open boxes) profiles are shown separately. There is often a typical cloud base level, above which the frequency of clear conditions rapidly deteriorates. This transition is most distinctive at night.